Up-to-date p-p Interaction Modeling and Secondary γ, $e^{\pm}$ and Neutrino Spectra in Astronomical Environment

Tuneyoshi Kamae*, Niklas Karlsson†, Tsunefumi Mizuno‡, Toshinori Abe§ and Tatsumi Koi
Stanford Linear Accelerator Center, Stanford University, Menlo Park, CA 94025, USA¶

We have calculated spectra of stable secondary particles (γ, $e^{\pm}$, ν_e, $\bar{\nu}_e$, ν_μ, and $\bar{\nu}_\mu$) produced in high energy p-p interactions in astrophysical environment. The calculation has incorporated the up-to-date rising inelastic cross-sections, the diffraction dissociation process, and the Feynman scaling violation for the first time. We then found that the diffractive process makes secondary particle spectra harder than that of the incident proton; that the rising inelastic cross-section and the scaling violation produces significantly more secondary particles than previous calculations. Combination of the three features explain about a half of the "GeV Excess" in the EGRET Galactic diffuse γ-ray spectrum with the local cosmic proton spectrum (power-law index around 2.7). The excess can be fully explained if the proton spectral index in the Galactic ridge is harder by 0.2 than above. As an extension of the calculation, we have parameterized the inclusive secondary particle spectra as functions of the incident proton kinetic energy: we predict $\sim 30\%$ more e^+ and ν_e than e^- and $\bar{\nu}_e$ to be produced in the GeV range by p-p interactions.

1. Introduction

Through numerical simulation of $pp \to \pi^0$ process to account for the Galactic diffuse γ-ray emission observed by EGRET[1], three off the authors came to note that all past calculations [2–8] had left out an important component of inelastic p-p interaction, the diffractive interaction, nor incorporated the Feynman scaling violation in the non-diffractive inelastic interaction. Another important finding was that these calculations had assumed a energy-independent p-p inelastic cross-section of ~ 24 mb for $T_p \gg 10$ GeV. Updating these shortfalls is likely to change the γ-ray and other secondary particle spectra (eg., $e^{\pm}$ and neutrinos) produced in the proton ISM interaction: the diffractive process will add secondary particles in the highest end of the spectrum; the scaling violation and the up-to-date inelastic cross-section will increase the particle yields in the GeV range.

We simulated the p-p inelastic interaction separately for the non-diffractive and diffractive processes. The non-diffractive process is calculated by two computer programs: Pythia 6.2 [9] for the proton kinetic energy (T_p) range 512 TeV $\geq T_p \geq$ 52.6 GeV and a parametrized model by Blattnig et al [10] for 52.6 GeV $\geq T_p >$ 0.488 GeV. The diffractive process is simulated by a program written by one of the authors on the formulae given in literature [11–13].

To track down the changes the updatings bring in, we use two models of inelastic p-p interaction: model A incorporates all three features and hence is the most up-to-date modeling; model B approximates the old scaling models within our choice of computer programs. We note that the legacy scaling models [2–8] and model B do not include the diffractive process nor the multi-parton level scaling violation [14, 15]. They, however, can differ up to $\sim 100\%$ among themselves when extrapolated to GeV energy range.

A part of this work has been published [16] and the remainder will be submitted for publication in near future.

2. Breakdown of the Inelastic Cross-Section

The total p-p cross-section is broken down to the elastic, non-diffractive inelastic, and diffractive inelastic cross-sections. The total and elastic cross-sections have been measured accurately and compiled by Hagiwara et al. [17]. They are plotted as experimental points in Fig.1a together with the cross-sections used in model A. The total inelastic cross-section is, by definition, the difference between the total and elastic cross-sections.

The diffractive inelastic process where the projectile proton and/or the target proton transition to excited states (discrete nucleon resonances and conituum) became known by early 1970's [18]. In the non-diffractive inelastic process, the two protons collide head-on and disrupt their quark-gluon structures. The early data led to a naive conjecture that the diffractive cross-section increases with the incident proton energy while the non-diffractive inelastic cross section stays constant at ~ 24 mb above ~ 10 GeV. According to recent studies, this conjecture is oversimplification and inaccurate. The increase in the to-

*Also with Kavli Institute for Particle Astrophysics and Cosmology, Stanford University
†Visiting scientist from Royal Institute of Technology, SE-10044 Stockholm, Sweden
‡Present address: Department of Physics, Hiroshima University, Higashi-Hiroshima, Japan 739-8511
§Present address: Department of Physics, University of Tokyo, Tokyo, Japan 113-0033
¶Electronic address: `kamae@slac.stanford.edu`

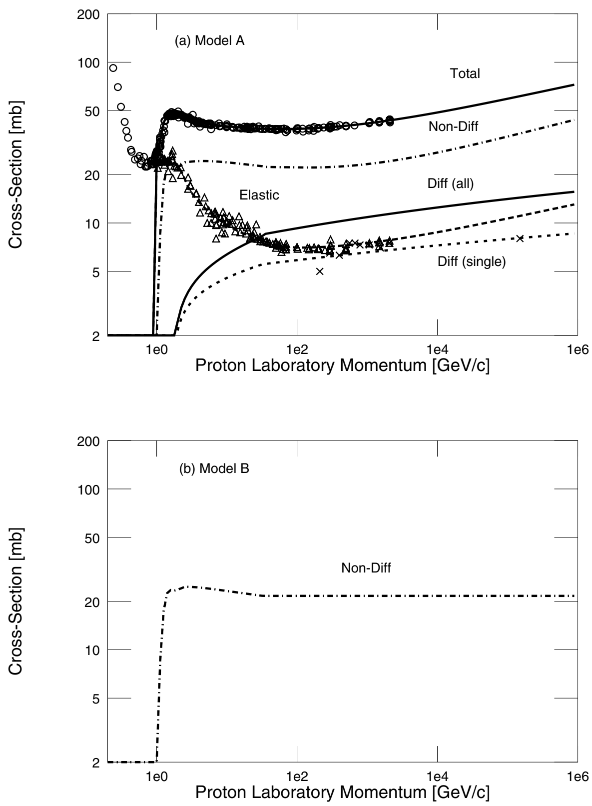

Figure 1: The p-p cross-section models: (a) for model A and (b) for model B. Curves are for the total (*upper solid*), non-diffractive inelastic (*dot-dashed*), elastic (*dashed*), all diffractive (*lower solid*), and single diffractive (*dotted*) processes. Note that model B is made only of non-diffractive inelastic process. Data are for the total (*circles*), elastic (*triangles*), and single diffraction (*crosses*).

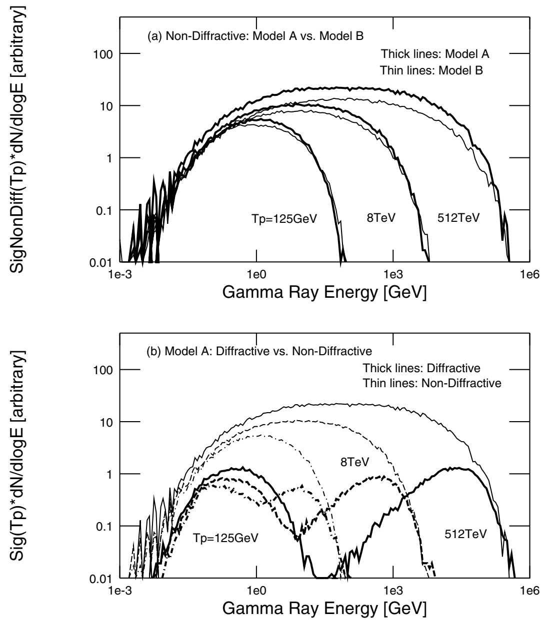

Figure 2: Predicted gamma-ray spectra for 3 mono-energetic proton beams: (a) the non-diffractive contribution in model A (*thick lines*) and model B (*thin lines*); and (b) the non-diffractive in model A (*thick lines*) and diffractive in model A (*thin lines*). Proton kinetic energies (T_p) are 512 TeV (solid), 8 TeV (*dashed*), and 125 GeV (*dot-dashed*). Note that model A generates $30 - 80$ % more multi-GeV gamma-rays for $T_p > 100$ GeV.

tal cross-section is shared by the non-diffractive and diffractive processes as incorporated in model A and shown in Fig.1a [12, 13, 20]. Fig.1b depicts the model B non-diffractive inelastic cross-section: the diffractive process is left out as has been in all previous predictions on the diffuse Galactic gamma-ray spectrum [2–8].

The contribution of the rising non-diffractive cross-section and scaling violation to the gamma-ray spectrum can be read off as the difference in the 2 curves in Fig.2a. The non-diffractive and diffractive contributions are compared in Fig.2b. The effect of the former on the γ-ray spectrum (and other secondary particle spectra) is increase in the yield over the entire spectrum of about $10 - 60\%$ for protons wiht $T_p > 100$ GeV. That of the diffractive process is adding an appreciable amount of γ-rays (and other secondary particles) at the highest and lowest ends of the spectrum.

3. Gamma-Ray Spectra by p-p Interactions in the Galactic Ridge

In Fig.3, the γ yields from the non-diffractive and diffractive processes are summed between $T_p =$ 0.488 GeV and 512 TeV with weights corresponding to power-law spectrum of Ind=2.0 (a), a broken power-law representing the Local Intersteller Spectrum (b:LIS), and another broken power-law of Ind=2.2/2.5 ($T_p < / > 20$ GeV) (c:Trial4GR). Models A and B are represented by solid and dashed curves, respectively. We note in Fig.3 that the γ-ray spectra predicted by model A are significantly harder than the incident proton spectrum: the difference amount to a factor of two for Ind=2.0 at around 50 TeV.

The EGRET count and exposure maps for the observation period 1-4 have been downloaded from the EGRET archive. All point sources listed in the EGRET 3rd Catalog [19] are then removed using the point-spread function of EGRET for each energy band and for the power-law index of each point source listed in the catalog. The flux between 100 MeV and 10 GeV has been constrained to that of each point source listed in the EGRET 3rd Catalog. The point-source-subtracted count map is then divided by the corre-

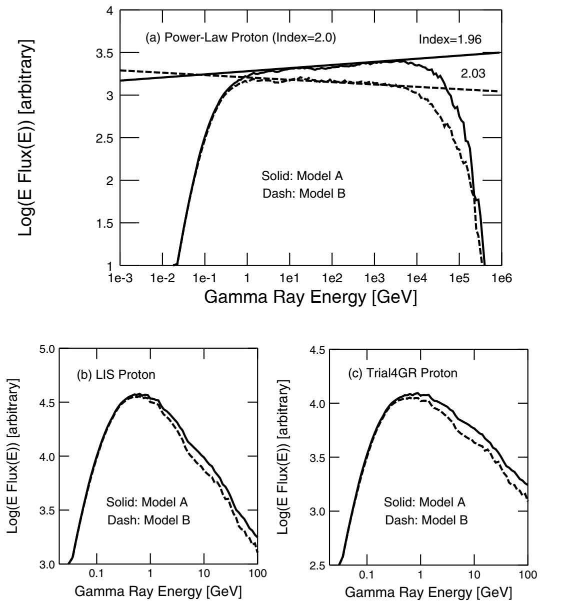

Figure 3: Gamma-ray spectra predicted for the 3 proton spectra between 0.488 GeV $< T_p <$ 512 TeV: (a) power-law with index=2.0, (b) LIS, and (c) Trial4GR. Curves are for model A (*solid*) and model B (*dashed*). Asymptotic power-law indices of gamma-ray spectra are: 1.96/2.03 (Index=2 model A/model B), 2.65/2.71 (LIS model A/model B), and 2.47/2.53 (Trial4GR Model A/Model B).

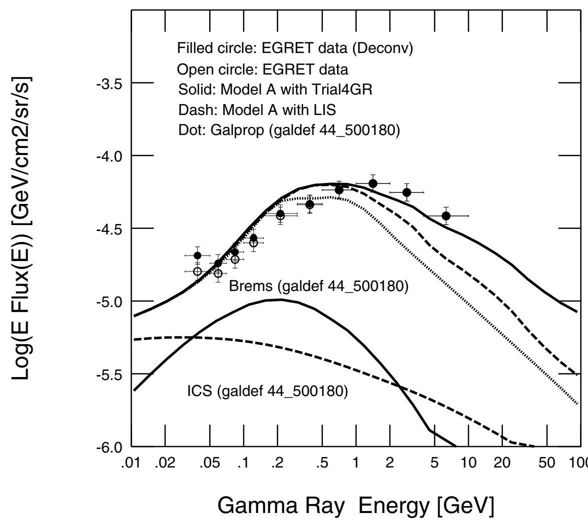

Figure 4: Model gamma-ray spectra including the contributions from bremsstrahlung and inverse-Compton and the EGRET data. Model curves are:(Brems) bremsstrahlung contribution; (ICS) inverse-Compton contribution, of GALPROP [22, 23] with parameters galdef 44_500180 by Strong, Moskalenko, and Rimer [24]. Other curves are: model A (Trial4GR)+Brems+ICS (*solid*); model A (LIS)+Brems+ICS (*dashed*); π^0+Brems+ICS by GALPROP with galdef 44_500180 [24] (*dotted*).

sponding exposure map to make the intensity map. The intensity between the Galactic latitude ±6.0 deg. and Galactic longitude ±30.0 deg has been summed and normalized to a unit solid angle to become our EGRET Galactic ridge spectrum used in this work. The point-source-subtracted intensity map has been checked to be consistent with the similar map given by Strong, Moskalenko and Rimer [21]. The intensity is then divided by the bin width and multiplied by E_{bin}^2, or the mid-energy squared. The results are shown by open circles with error bars in Fig.4.

A second EGRET spectrum has been calculated in the same manner as above except that the point-source-subtracted count map is processed further to deconvolve the point spread function (PSF): energy dependency of the PSF used in the deconvolution has been derived assuming a power-law incident gamma-ray (index 2.1). Details will be described in a separate publication (T. Kamae et al. 2005, in preparation). The deconvolution removes artifacts introduced by the broad EGRET PSF, in particular, for $E_\gamma <$ 150 MeV and allows us to compare the observed spectrum and model predictions directly. Thus obtained EGRET Galactic ridge spectrum (referred to as "deconvolved") are shown by filled circles with error bars in Fig.4.

We then combine the model A prediction with the bremsstrahlung and inverse-Compton spectra predicted by GALPROP [22, 23] with the conventional cosmic ray spectra (the parameter "galdef 44_500180" by Strong, Moskalenko, and Rimer [24]). Here we normalize the model A $\pi^0 \rightarrow \gamma$-ray spectra (with LIS and Trial4GR) to π^0 gamma-ray spectrum of this GALPROP model in the energy region $E_\gamma <$ 300 MeV. Since the contributions by pion decay, bremsstrahlung, and inverse Compton are mutually fixed within the GALPROP model, we add the model A (Trial4GR and LIS), the GALPROP bremsstrahlung, and the GALPROP inverse Compton to obtain the spectra labeled as "model A with Trial4GR" (*solid curve*) and "model A with LIS" (*dashed curve*). We note that the normalization to the EGRET data relative to the 3 models is still unconstrained and our focus should be on the spectral shape.

We note that the discrepancy in the GeV region or "GeV Excess" is reduced to about 50 % if we compare model A (LIS) and the GALPROP spectrum. The EGRET spectrum deconvolved of the point spread function improves agreement between the data and the models in the lower slope of the gamma-ray spectrum. The spectrum Trial4GR combined with model

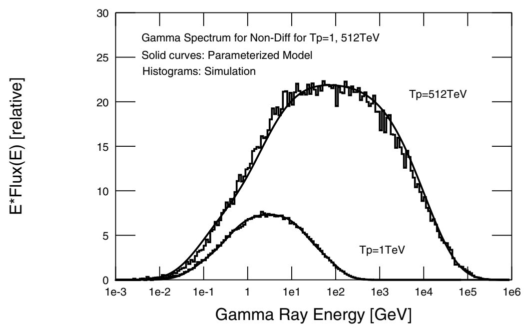

Figure 5: Parametrized non-diffractive γ-ray inclusive cross-section for $T_p = 1$ and 512 TeV. Histograms: simulations for mono-energetic protons, solid curve: the preliminary parameterized model defined by Eq.1, Eq.2, and Table 2.

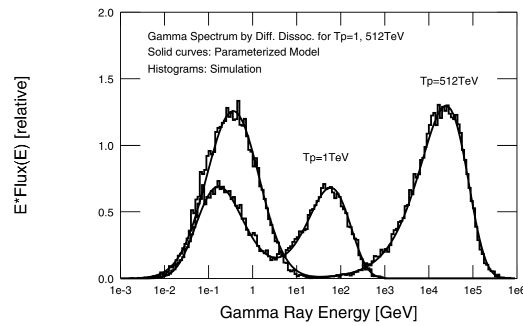

Figure 6: Parametrized diffractive γ-ray inclusive cross-section for $T_p = 1$ and 512 TeV. Histograms: simulations for mono-energetic protons, solid curve: the preliminary parameterized model defined by Eq.1, Eq.2, and Table 2.

A (Fig.4, *solid curve*) produces a $E_\gamma^2 F(\gamma)$ consistent with EGRET data in GeV range.

4. Paramaterization of Secondary Particle Spectra

4.1. Paramterized γ-ray Spectra

To facilitate the use of the present model (model A) in predicting proton-induced secondary fluxes and spectra in astrophysical environments (eg. Galactic ridge, AGN jets, SNR shock fronts, local galaxies, and galaxy clusters), we have parameterized particle yields as functions of incident proton enery. The parameterization has been done in the following steps: (1) Fit the secondary particle spectra for mono-energetic protons at a sequence $T_p = 1000.0 \times 2^{(N-22)/2}$ GeV where $N = 0 - 40$ by eq.1 (non-diffractive) and eq.2 (diffractive).

The parameterization formulae for γ-ray are given by Eq.1, Eq.2 and Table 1 for non-diffractive and diffractive processes separately. Table 2 gives preliminary results on T_p dependence of these parameters. The formulae reproduce non-diffractive and diffractive simulation results reasonable well for mono-energetic protons as shown in Figs.5 and 6 for $T_p = 1$ and 512 TeV. Regarding the T_p dependence of the parameters given in Table 2, finer tuning is still being done so that: energy-weighted energy flux ($E \times Flux(E)$) will not blow-up at highest energies for power-law spectra with varying indices (eg. between 2.0 and 3.0); the continuum spectra will not introduce artifact wiggling. Fig.7 gives the γ-ray spectrum obtained on the preliminary parameterized model for power-law protons of index 2.0: we find subtle dent in the middle of the spectrum which needs to be improved.

$$\begin{aligned}&\Delta\sigma(\gamma)[\mathrm{mb}]/\Delta\log(\mathrm{E}_\gamma)(5\%\mathrm{bin}) = \\ &a_0 exp(-a_1(x-a_3+a_2(x-a_3)^2)^2) + \\ &a_4 exp(-a_5(x-a_8+a_6(x-a_8)^2+a_7(x-a_8)^3)^2)\end{aligned} \tag{1}$$

$$\begin{aligned}&\Delta\sigma(\gamma)[mb]/\Delta log(E_\gamma)(5\%\mathrm{bin}) = \\ &b_0 exp(-b_1((x-b_2)/(1.0+b_3(x-b_2)))^2) + \\ &b_4 exp(-b_5((x-b_6)/(1.0+b_7(x-b_6)))^2)\end{aligned} \tag{2}$$

4.2. Paramterized $e^\pm$ and Neutrino Spectra

Model A for γ-ray has been extended to simulate other secondary particles, $e^\pm$, ν_e, $\bar{\nu}_e$, ν_μ, and $\bar{\nu}_\mu$. Secondary spectra produced by power-law protons of index 2.0 (0.488 GeV $< T_p <$ 512 TeV have been computed on the model as shown in Fig.8 ($e^\pm$) and Fig.9 (ν_e $\bar{\nu}_e$, ν_μ, and $\bar{\nu}_\mu$). We note in Fig.7 that more e^+ are produced than e^- because of the charge conservation: the law operated very effectively at lower energy and for the diffractive process where multiplicity of particles produced is expected to be low. The charge conservation law reflects itself to favor ν_e over $\bar{\nu}_e$ through the lepton number conservation law as seen in Fig.9.

5. Conclusion and Future Prospects

We conclude that an up-to-date modeling of the *p*-*p* interaction (model A) with the diffractive process and the Feynman scaling violation makes the gamma-ray

Table I Parameters describing γ spectra for mono-energetic proton beams

Parameters	$T_p = 1$ TeV	$T_p = 512$ TeV
Eq. 1		
a_0	3.739	12.16
a_1	7.0116e-06	2.462e-06
a_2	-242.98	-135.33
a_3	0.8266	2.257
a_4	3.556	9.561
a_5	4.858e-06	1.746e-06
a_6	-267.83	-143.96
a_7	-28.96	0.5162
a_8	0.1609	1.2603
Eq. 2		
b_0	0.70148	1.2674
b_1	1.6588	1.3710
b_2	-0.7660	-0.4553
b_3	0.15960	-0.01856
b_4	0.6755	1.3120
b_5	2.1630	1.6672
b_6	1.7656	4.4037
b_7	-0.1526	-0.24130

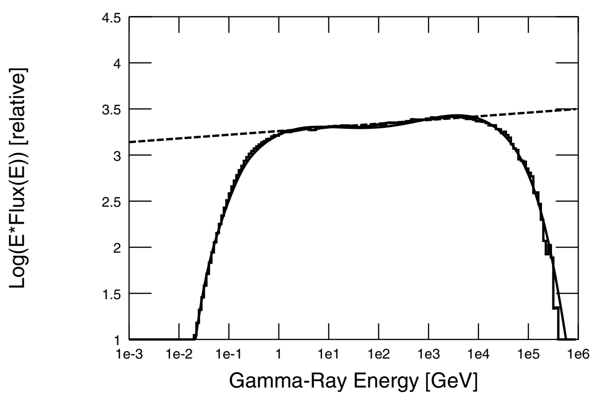

Figure 7: Gamma-ray spectrum produced by protons with power-law spectrum of index=2 by the preliminary parametrized model defined by Eq.1, Eq.2, and Table 2. The dashed straight line corresponds to index of 1.96.

spectrum harder and produces 30−80% more gamma-rays (Figs.3 and 4) than previous predictions [2–8] for incident protons with $T_p > 100$ GeV. Combination of the two can explain ~ 50 % of the "GeV Excess" in the EGRET Galactic ridge spectrum within the conventional cosmic proton and electron spectra as shown in Fig.4. The above statement is only relative to other $pp \to \pi^0$ production models: the absolute prediction of the Galactic ridge gamma-ray spectrum is contingent on the absolute normalization, or the

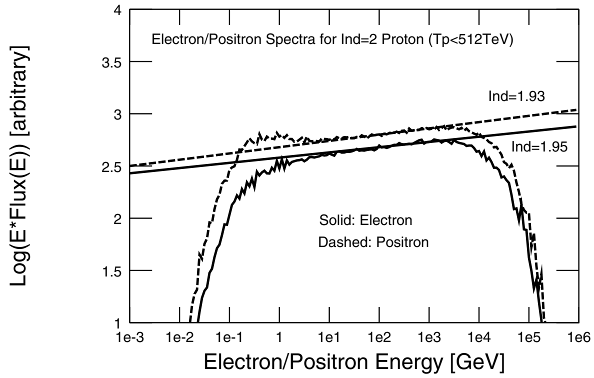

Figure 8: Electron and positron spectra produced by protons with power-law spectrum of index=2 by model A. The solid and dashed straight lines correspond to indices of 1.95 and 1.94, respectively.

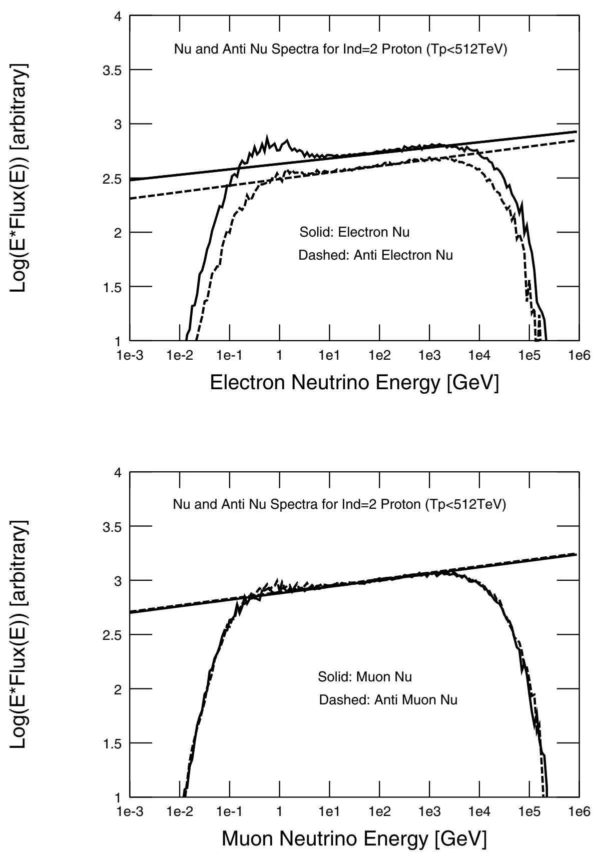

Figure 9: Neutrino spectra produced by protons with power-law spectrum of index=2 by model A. Upper panel: electron neutrino and electron anit-neutrino. The solid and dashed lines correspond to indices of 1.95 and 1.94, respectively. Lower panel: muon neutrino and muon anit-neutrino. The solid and dashed lines correspond to index of 1.94.

Table II Parameters describing gamma-ray spectra for arbitrary proton energy

Parameters	Formulae as functions of the proton kinetic energy ($y = T_p$) in GeV.
	Parameter values given here are still preliminary.
Eq. 1	
a_0	$-0.1518(y+3.4) + 0.9296(y+3.4)^2 - 0.2512(y+3.4)^3 + 0.02549(y+3.4)^4$
a_1	$7.199 \cdot 10^{-6} - 4.210 \cdot 10^{-6} y + 3.065 \cdot 10^{-7} y^2 + 3.935 \cdot 10^{-7} y^3 + 1.504 \cdot 10^{-7} y^4 - 7.513 \cdot 10^{-8} y^5$
a_2	$-191.9 + 173.9 \log_{10}(1.350(y+3.4)) - 747.0/(y+4.598)$
a_3	$0.8013 + 0.5324y + 0.01011y^2$
a_4	$0.6361(y+3.4) + 0.2815(y+3.4)^2 - 0.08064(y+3.4)^3 + 0.0100(y+3.4)^4$
a_5	$-5.875 \cdot 10^{-7} - 1.399 \cdot 10^{-6} \log_{10}(0.2139(y+3.4)) + 1.296 \cdot 10^{-4}/(y+4.736)^2$
a_6	$-3.411 \cdot 10^2 + 6.193 \cdot 10^2 \log_{10}(0.3173(y+3.9)) + 2.685 \cdot 10^2/(y+4.502)^2$
a_7	$1.024 \cdot 10^4 - 9.888 \cdot 10^3 \log_{10}(0.2976(y+12.0)) - 2.872 \cdot 10^6/(y+24.44)^2$
a_8	$0.1580 + 0.3861y + 4.322 \cdot 10^{-3} y^2$
Eq. 2	
b_0	$6.065 \tanh(-0.3597(y+2.2)) - 0.5605(y+0.5384)^2 + 5.282 \cdot 10^{-4}(y+9.789)^4$
b_1	$-295.5 + 308.6 \exp(-10.60((y+2.083)/(1.0+16.33(y+2.083)))^2)$
b_2	$-16.19 - 0.07540 \tanh(-1.675(y+2.1)) - 2.380 \cdot 10^{-4}(y+2.549 \cdot 10^2)^2$
b_3	$-5.702 \cdot 10^2 + 5.704 \cdot 10^2 \exp(-2.031 \cdot 10^{-4}((y+1.263)/(1.0+0.4684(y+1.263)))^2)$
b_4	$0.4297 + 4.976 \cdot 10^{-2}(y+2.2)^2 - 6.628 \cdot 10^{-4}(y+2.2)^4 + 7.738 \cdot 10^{-2} \log_{10}(y+2.2)$
b_5	$2.164 - 0.2116y - 0.02482y^2 + 0.03459y^3 - 7.431 \cdot 10^{-3} y^4$
b_6	$1.769 + 0.9516y + 2.111 \cdot 10^{-2} y^2 + 1.560 \cdot 10^{-2} y^3 - 7.873 \cdot 10^{-3} y^4$
b_7	$-0.1645 - 0.1212y + 3.464 \cdot 10^{-2} y^2 - 0.4263 \exp(-0.7386(y+1.859)^2)$

absolute cosmic ray fluxes, the absolute ISM density, and the absolute radiation field density. As far as the gamma-ray spectral shape is concerned, the remaining discrepancy in Fig.4 requires some modification to the conventional cosmic ray spectra: one possibility is to assume the proton spectrum in the Galactic ridge to be a little harder than that of the solar neighborhood, eg. ~ 2.5 in power-law index as Trail4GR in Fig.4.

We have produced a parameterized model (preliminary) for the yield and spectrum of γ-rays produced in p-p interaction. We have extended model A to predicted the $e^{\pm}$ and neutrino spectra of proton origin. Through these works, we found:

- The up-to-date rising cross-section, diffractive interaction and scaling violation (model A) makes secondary particle spectra harder than the incident proton spectrum. Their yields nearly double at multi-GeV energy for power-law protons with index=2.0, compared with those by model B, our approximation to the scaling model.
- Combination of the inherently low multiplicity, we expect more e^+ than e^- and more ν_e than $\bar{\nu_e}$ from p-p interaction as shown in Figs. 8 and 9. Depending on the primary e^- and e^+ fluxes at the astronomical environment of interest, the e^+ excesse may become observable at higher energies.

We are currently building parameterized models for e^-, e^+, and neutrinos. That for γ-ray presented here is still preliminary. The results will be published in near future. We have neglected contributions of α particles and helium atoms/ions to the gamma-ray spectrum. We intend to include p-n interaction in the publication.

6. Acknowledgments

One of us (Kamae) would like to acknowledge valuable discussions with Igor Moskalenko, Andy Strong and Dino Goulianos. Moskalenko and Strong kindly made the GALPROP program and galdef parameters available to him. Goulianos directed him to several references. The authors thank advice and assistance given by D. Elwe, J. Chiang, S. Digel, I. Grenier, P. Kunz, G. Madejski, H. Tajima P. Nolan, R. Hartman, S. Hunter, M. Mori, J. Ormes, F. Stecker, D. Thompson, M. Asai, N. Graf and Y. Shimizu.

References

[1] Hunter, S.D., et al. 1997, ApJ, 481, 205
[2] Stecker, F. 1970, Astro and Space Science 6, 377
[3] Stecker, F. 1973, ApJ, 185, 499
[4] Strong, A.W., et al. 1978, MNRAS, 182, 751
[5] Stephens, S.A., and Badhwar, G.D. 1981, Astrophys. Space Sci, 76, 213

[6] Dermer, C. D. 1986, A&A, 157, 223

[7] Stecker, F. 1989, in Shapiro, M.M., and Wefel, J.P. (eds.), “Cosmic Gamma Rays, Neutrinos and Related Astrophysics”, p.89

[8] Mori, M. 1997, ApJ, 478, 225

[9] Sjöstrand, T., Lonnblad, L., and Mrenna, S. 2001, “Pythia 6.2: Physics and Manual”, hep-ph/0108264

[10] Blattnig, S. R., et al. 2000, Phys. Rev., D62, 094030

[11] Goulinanos, K. 1983, Phys. Reports, 101, 169

[12] Goulinanos, K. 1995, Phys. Lett., B358, 379

[13] Goulinanos, K., and Montanha, J. 1999, Phys. Rev., D59, 114017

[14] Field, R.D. 2002, Matrix Element and Monte Carlo Tuning Workshop, $http://cepa.fnal.gov/CPD/MCTuning$, $http://www.phys.ufl.edu/\ rfield/cdf$

[15] Sjöstrand, T., and Skands, P. Z. 2004, hep-ph/0402078

[16] Kamae, T., Abe., T, & Koi, T., 2005, ApJ 620, 244

[17] Hagiwara, K., et al. 2002, Phys. Rev., D66, 010001.

[18] Alberi, G., and Goggi, G. 1981, Phys. Reports, 74, 1

[19] Hartman, R.C., et al. 1999, ApJ, 123, 79

[20] Affolder, T., et al. 2001, Phys. Rev. Lett., 87, 141802

[21] Strong, A. W., Moskalenko, I. V., and Reimer, O. 2000, ApJ, 537, 763; Errortum: 2000, ibid, 541, 1109

[22] Strong, A.W., and Moskalenko, I.V. 1997, Proc. Fourth Compton Symp., (eds) Dermer, C. D., Strickman, M. S., and Kurfess, J. D., p.1162; astro-ph/9709211

[23] Strong, A. W., and Moskalenko, I. V. 2001, Proc. of 27th ICRC 2001 (Hamburg), p.1942 and astro-ph/0106504

[24] Strong, A. W., Moskalenko, I. V., and Reimer, O. 2004, ApJ, 613, 962